Discharge Characteristics and Non-Spectral Interferences on the Emission of Ca Species in a Medium Power Radiofrequency Capacitively Coupled Plasma Source

Tiberiu Frentiu,[1],* Michaela Ponta,[1] Eugen Darvasi,[1] Maria Frentiu[2] and Emil A. Cordos[2]

[1] *Babes-Bolyai University, Faculty of Chemistry and Chemical Engineering, Arany Janos 11, 400028 Cluj-Napoca, Romania*

[2] *National Institute for Research and Development of Optoelectronics Bucharest – Research Institute of Analytical Instrumentation, Donath 67, 400293 Cluj-Napoca, Romania*

* Corresponding author: E-mail: ftibi @chem.ubbcluj.ro
Tel.40264 593833; Fax: 40264 590818

Abstract

Non-spectral interference of easily ionized elements (EIEs) as chlorides and Al as $AlCl_3$ and $Al(NO_3)_3$ on the emission of Ca II 393.367 nm, Ca I 422.673 nm, CaOH 554 nm and 622 nm were studied in a medium power radiofrequency capacitively coupled Ar plasma (275 W, 27.12 MHz) with single (SRTrfCCP) and double ring electrode (DRTrfCCP). The mechanisms of interferences were explained based on the matrix energy demand (MED) supposing the local thermal equilibrium (LTE) in plasma, emphasizing also processes contrasting with this model. Matrix effects were found to be dependent on the coupling geometry of the rf power to the torch, observation height, emitting Ca species and EIEs matrix nature but independent from Al as regards its salt origin. The magnitude of the matrix effects was correlated with the electron number density and the discharge temperature. The optimization of the observation height and use of the DRT geometry allowed the reduction of EIEs and Al matrix effects on the emission of Ca species compared to SRT. The best Ca detection limits in SRTrfCCP were at CaOH 622 nm (106–450 ng ml^{-1}), while in DRTrfCCP at Ca I 422.673 nm (92–145 ng ml^{-1}).

Keywords: Radiofrequency capacitively coupled plasma, optical emission spectrometry, non-spectral interference, Ca determination

1. Introduction

Although more than 60 years passed since the beginning study about the possibility to use the radiofrequency capacitively coupled plasmas (rfCCPs) in spectrochemical analysis,[1] these have returned in the attention of analytical community as a result of their advantages: low power and gas consumption, good sensitivity for a number of analytical applications, low cost and easy operation. RfCCPs can be developed in different geometries[2–9] within a large range of power (5–300 W) at atmospheric pressure with gas consumption between 5 mL min^{-1} – 1 L min^{-1}. The versatility of the rfCCPs for spectrochemical analysis has been proven for liquid[10–12] and direct conductive or non-conductive solid samples.[13,14] The advantages associated to sensitivity in the analysis of clinical microsamples by electrothermal vaporization without digestion,[15] the specificity as detector in gas chromatography for organometallic[16] and toxic halogenated compounds,[17–19] and the possibility to interface with vapor generator for Hg, Sb and As determination by emission[6] were emphasized in the literature. Despite these advantages, the non-spectral interferences of easily ionized elements (EIEs) represent a certainty in low and medium power rfCCPs and consequently they have been extensively studied.[10, 15, 20–26] Besides the capability in multielemental determination, a spectral source should be free from spectral and non-spectral interferences in order

to be considered as ideal for optical spectroscopy. When such interferences are present, it is important to recognize and control their extent. Non-spectral interferences directly affect the analyte signal either by altering atoms concentration in the plasma or changing the plasma characteristics or both in some cases.[20]

The rfCCP torch with single or double ring electrode (SRTrfCCP and DRTrfCCP) operated at 275 W developed in our laboratory[27] has proved to be a valuable tool in the multielemental determination by optical emission spectrometry (OES) of environmental, biological and superconducting materials.[12,28–34] Besides the relatively good excitation capability, the SRTrfCCP was recently reported for the first time as a promising atomization cell for Cd fluorescence spectrometry.[35]

Determination of elements by OES and the associated non-spectral interferences in low and medium power plasmas have been extensively studied in the literature rather at the atomic lines than at ionic lines and molecular bands. For this kind of plasmas it appears as useful to explore the determination of some analites at their molecular bands, since low/medium power plasma sources are not capable to dissociate refractory compounds. From the fundamental perspective, the objective of this study was to provide an almost complete picture of the non-spectral interferences in OES in a medium power plasma source due to EIEs and Al on Ca atomic and ionic lines, and molecular bands and the linkage to the discharge characteristics. Calcium was selected in the study as it develops relatively easily atomic and ionic but also refractory molecular species and exhibits both ionization and solute vaporization interferences. The mechanism of non-spectral interference of EIEs as LiCl, NaCl, KCl and of aluminium as $AlCl_3$ and $Al(NO_3)_3$ on the optical emission at Ca II 393.367 nm, Ca I 422.673 nm and molecular bands CaOH 554 and 622 nm was studied in Ar SRTrfCCP and DRTrfCCP operated at 275 W. The investigated matrix effects were explained based on the matrix energy demand (MED)[36] supposing the local thermal equilibrium (LTE)[37] in plasma and correlated with the discharge temperature considered to be the rotational temperature of OH species (T_{rot}) and electron number density (n_e), respectively. The interferences were also correlated with torch configuration, observation height in the plasma and nature of Ca species in order to achieve the best figures of merit for Ca determination by OES using rfCCP with ring electrodes. This study is a matter of significant relevance for analytical practice of Ca determination, since EIEs and Al are present in a wide variety of natural matrices.

2. Experimental

2. 1. Stock Solutions and Reagents

Stock solutions of Ca, Na, Li, K and Al (1000 μg mL^{-1}) in 1 % (v/v) HNO$_3$ 69 % were prepared starting

from p.a or purum p.a $Ca(NO_3)_2 \cdot 4H_2O$, NaCl, LiCl, KCl, $AlCl_3 \cdot 6H_2O$ and $Al(NO_3)_3 \cdot 9H_2O$. Solutions of 10 μg mL^{-1} Ca in the presence of 0–500 μg mL^{-1} Li, Na, K and Al were used in the evaluation of non-spectral interferences. Argon (5.0 quality) from Gas SRL Cluj-Napoca, Romania was used as plasma support gas.

2. 2. Instrumentation

Measurements were performed by interfacing the rf-CCP generated in two geometric configurations (SRT, DRT) with two spectrometers. A multichannel spectrometer equipped with a photodiode array detector (PDA) was used in the study of non-spectral interferences and limit of detection. A high-resolution scanning spectrometer was used to record the OH spectra and evaluate the ionic-to-atomic emission ratio of Ca species in the study of physical characteristics of plasma. The experimental set-up of the DRTrfCCP interfaced with the multichannel spectrometer is presented in Figure 1 and Table 1. A detailed drawing of the torch in the SRT and DRT version was previously presented.[27]
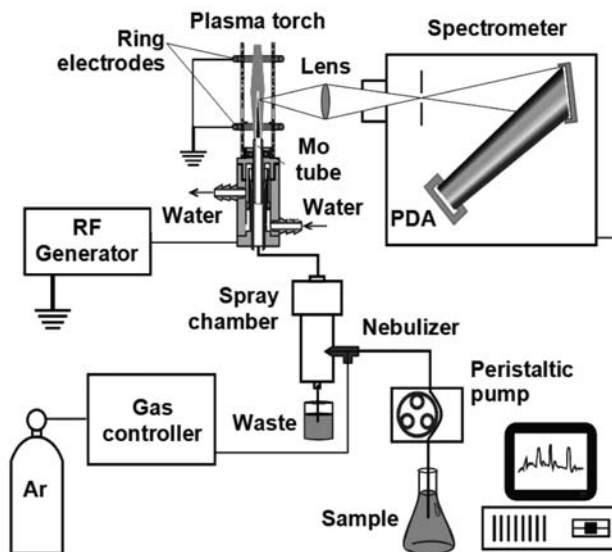

Figure 1: Block diagram of the experimental set-up of DRTrfCCP-OES equipped with PDA multichannel spectrometer

3. Results and Discussion

3. 1. Discharge Characteristics

The discharge temperature considered to be the rotational temperature (T_{rot}) of molecular radicals was determined from the negative slope of the Bolzmann plot using spectral data for OH band emission given in Table 2.[38]

The lines were selected from the R branch in the origin vicinity of the OH molecular band 308.90 nm ($A^2\Sigma^+$, ν

Table 1: Instrumentation and operating conditions of spectrometric systems (INCDO-INOE 2000, Research Institute for Analytical Instrumentation, Cluj-Napoca, Romania)

Equipment	Characteristics
Plasma power supply	Rf Generator, 275 W, free-running oscillator, 27.12 MHz
Plasma torch	Ar capacitively coupled plasma (0.4 L min⁻¹) with central Mo tubular electrode (i.d. 3.5 mm) connected to the rf generator and operated in two configurations: (a) coaxial with single ring electrode (SRT) at 5 mm above the tubular electrode (b) coaxial-annular with double ring electrode (DRT) spaced at 60 mm
Sample introduction system	Concentric pneumatic nebulizer equipped with peristaltic pump and Scott spray chamber. Sample intake into the core of the plasma through the tubular electrode (1 mL min⁻¹, 5 % nebulization efficiency).
Optics for the study of non-spectral matrix effect	Multichannel spectrometer equipped with PDA detector, Paschen-Runge mount, 200–1100 nm spectral range, 95 mm focal length, 133 grooves mm⁻¹ grating blazed at 330 nm, 8 nm spectral bandpass. PDA detector type S3904-512Q MOS linear image sensor, 512 photodiodes, 25 × 2500 μm sensitive area.
Optics for the study of physical characteristics	190–800 nm high-resolution scanning spectrometer, 1 m Czerny-Turner mounting, 2400 groves mm⁻¹ grating blazed at 330 nm, 20 μm slits width, EMI 9781R photomultiplier tube.

Table 2: Spectral data for OH band emission[38]

| λ(nm)	E_J (eV)	$\nu_{JJ'}$ (cm⁻¹)	$S_{JJ'}$	Spectroscopic branch
307.114	4.453	35913.21	53.2	$R_2(14)$
307.303	4.512	36394.95	57.2	$R_2(15)$
307.437	4.064	32778.99	12.8	$R_2(4)$
307.703	4.047	32643.83	9.1	$R_2(3)$

$= 0 \to X^2\Pi, \nu = 0$) as they provide a better quantify uncertainty in T_{rot} measurement for several reasons. Their frequency uncertainty is lower than for lines belonging to the P branch, and the lines having high and low rotational quantum numbers are less prone to self-absorption, and consequently their intensities can be more accurately measured. Moreover, the narrow spectral range of the selected lines eliminates the need of emission signal correction according to the detector response curve, which could be a source of uncertainty in the temperature measurement.

The n_e was estimated from the Ca ionic-to-atomic intensities ratio and Boumans and De Boer[39] equation valuable in the LTE model. Data for n_e measurement are given in Table 3.[40]

The dependence of the T_{rot} of OH species and n_e on the observation height in SRTrfCCP and DRTrfCCP in the presence and absence of 100 μg mL⁻¹ Na as NaCl is

Table 3. Spectroscopic data for Ca lines[40]

Line	λ (nm)	E_{ex} (eV)	E_i (eV)	gA 10⁸ (s⁻¹)
Ca I	422.673	2.932	6.11	6.54
Ca II	393.367	3.152	–	5.88
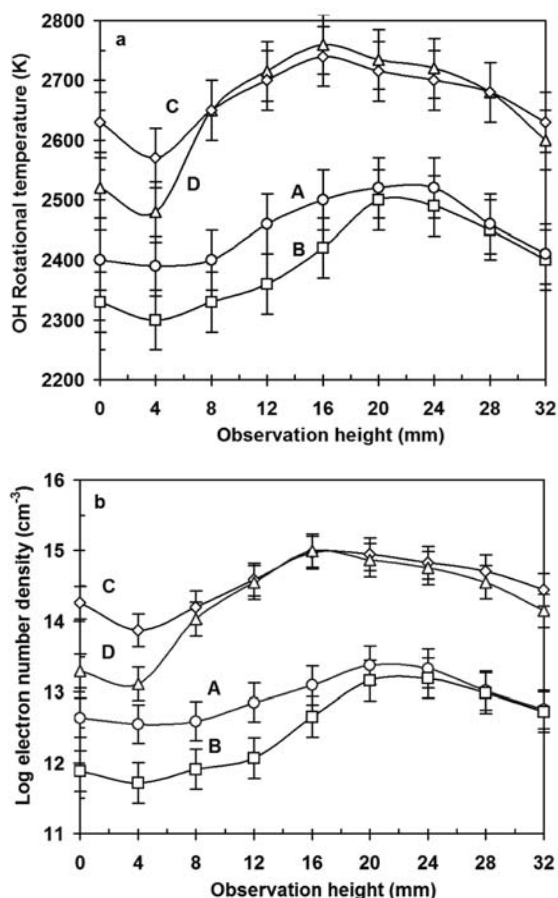
Figure 2: Rotational temperature of OH species (a) and electron number density (b) in SRT rfCCP in the absence (A) and presence of 100 μg mL⁻¹ Na matrix (B), and DRTrfCCP in the absence (C) and presence of 100 μg mL⁻¹ Na matrix (D).

shown in Figure 2ab. The error bars of T_{rot} correspond to an uncertainty of ± 50 K calculated from the standard deviation of the slope in the Bolzmann plot, while the error bars for n_e are related to the uncertainties of T_{rot} and ionic-to-atomic Ca emission intensities ratio.

Figure 2 indicates a dependence of the discharge temperature and n_e on the torch coupling geometry and a distribution of these parameters over the height in plasma, respectively. The plasma in the DRT configuration is hotter than in the SRT one, which is reflected in the higher rotational temperature of OH species both in the absence and presence of NaCl matrix. Even considering the uncertainty in temperature measurement, a cooling of the SRT plasma up to 16 mm height in the presence of NaCl is a certainty caused by the additional energy consumption by the matrix. In the DRT geometry the cooling occurs only below 4–6 mm. The electron number density is two orders of magnitude greater in the DRT plasma than in the SRT one as a consequence of the higher density of ionic species, which results in a higher ratio of Ca ionic-to-atomic emission intensities. Due to the more evident drop in temperature and the larger decrease of n_e in the SRT plasma when introducing NaCl solution, one can expect that the matrix effect on the emission of different Ca species to be more prominent than in the DRT plasma configuration.

3. 2. Matrix Effects of EIEs

The non-spectral matrix effects of NaCl in SRT and DRT plasmas *versus* observation height are shown in Figure 3a,b.

In the SRT plasma, the greater matrix effect of NaCl on the emission intensity occurs for observation heights below 22 mm as a result of plasma cooling and decrease of n_e. The depressive effect on the emission of ionic (curve A) and atomic species (curve B) and the enhancing one on that of CaOH molecular species (curves C, D) suggest that in the presence of NaCl matrix the SRT plasma is no

longer capable to accomplish the atomization of Ca compounds and excitation of its atoms and ions. Also, a recombination of Ca atomic and ionic species with OH radicals in the gaseous phase is favored by lower temperature.[41] Therefore, the EIE matrix effects in the SRT plasma could be explained using the LTE model and taking into account MED.

According to Figure 3b, there are two distinct zones along the DRT plasma in relation with the trend of the matrix effect, which shows the different involvement of matrix in the process of atomization-ionization equilibrium and excitation of the analyte species. In the zone below 6 mm, the enhancing matrix effect is more obvious for the molecular bands (curves C, D) than for ionic and atomic lines (curves A, B). The mechanisms governing the processes in the lower zone of DRT plasma are similar to those in SRT and could be explained by the LTE approach and MED of a particular interferent. In this region, a fraction of the plasma energy is spent for the vaporization and excitation of EIEs, in agreement with a previous report of Cordos et al.,[27] who found at 6 mm height the emission maximum of these elements. Consequently, the atomization degree of Ca molecular species decreases due to plasma cooling in the presence of the matrix. The trend of the matrix effect at viewing heights above 6 mm can be neither explained using LTE approach nor correlated with MED of EIEs.

The non-spectral matrix effects of NaCl up to 500 µg mL⁻¹ Na in SRT (curves A1–D1) and DRT (A2–D2) plasmas on Ca emission are shown in Figure 4. A similar behavior was observed in the presence of LiCl and KCl, respectively. The increasing matrix effect up to 50 µg mL⁻¹ Na or K and 25 µg mL⁻¹ Li on the emission of all Ca species in the SRT plasma can not be explained based on MED. Experiments revealed a vertical distribution of the emission intensity of Ca species controlled by the EIE matrix concentration contrasting to the phenomenon in inductively coupled plasma (ICP).[42] In these diluted ma-
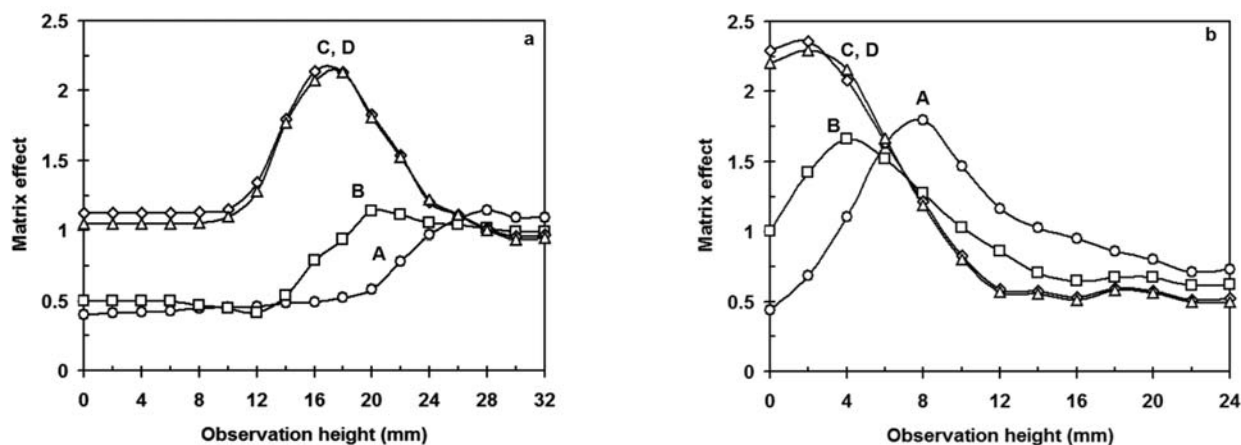

Figure 3: Matrix effect of 100 µg mL⁻¹ Na on Ca emission *vs.* observation height in SRT plasma (a) and DRT plasma (b) for Ca II 393.367 nm (A); Ca I 422.673 nm (B); CaOH 554 nm (C) and CaOH 622 nm (D).

trices the maximum emission occurs at lower observation height compared to matrix absence. The behavior is due to the diffusion interference, by which a concomitant with volatility greater than that of the analyte induces the increases of the vaporization speed of the solid particles and results in the development of molecular and atomic vapor cloud at lower heights in the plasma.[42]
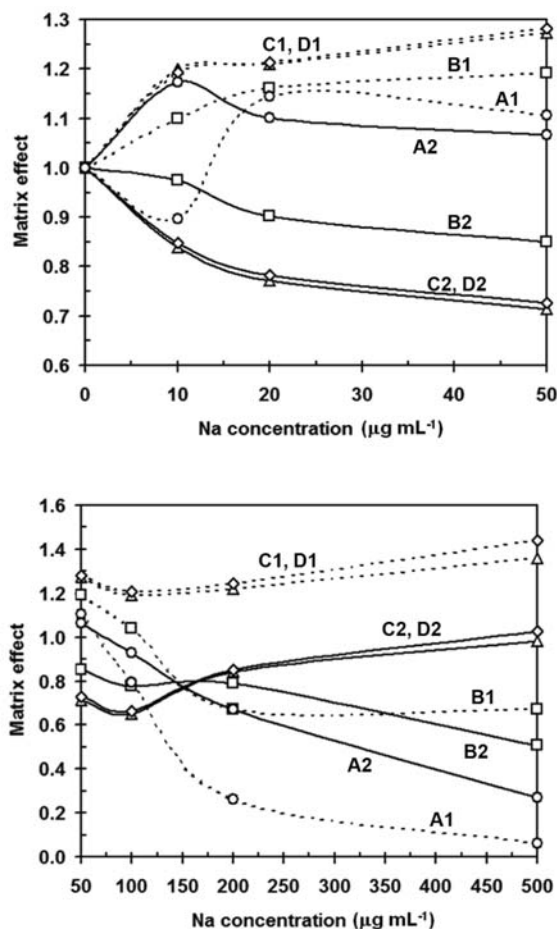

Figure 4: Effect of NaCl matrix concentration on Ca emission in SRT plasma (dotted line) and DRT plasma (solid line). A1, A2 – Ca II 393.367 nm; B1, B2 – Ca I 422.673 nm; C1, C2 – CaOH 554 nm and D1, D2 – CaOH 622 nm

For EIE levels over 50 µg mL⁻¹ Na or K and 25 µg mL⁻¹ Li, the maximum of the emission signal of Ca species shifts up as the matrix concentration increases, particularly at atomic and ionic lines. The reason is the supplementary MED causing a cooling of the SRT plasma, a decrease of n_e and recombination of Ca atoms with OH radicals. The result is the depressive matrix effect on the ionic (curve A1) and atomic emission (curve B1) and an increasing effect on the molecular bands (curves C1, D1).

Unlike SRT, in the DRT plasma, two trends can be observed depending on the matrix concentration. For concentrations below 100; 150 and 350 µg mL⁻¹ Li, Na and

K, the matrix effects do not obey the LTE model and the observed changes in the emission intensity can not be correlated with MED. Several additional mechanisms might be invoked to explain the increase of the atomic and ionic emission and the decrease of the molecular one. One reason could be the increase of the electrons energy through the direct charge transfer from an Ar ion to EIEs atom when an energy of 10.4–11.5 eV is gained. It corresponds to the difference between the ionization energies of Ar (15.76 eV) and EIEs (4.35–5.40 eV) respectively (Eq.1) and is carried off by a medium energy electron.

$$Me + Ar^+ + e_s^- \rightarrow Me^+ + Ar + e^-$$

$$\Delta E = 10.4 - 11.5 eV \qquad (3)$$

$$Me = Li, Na, K$$
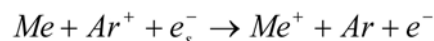
Therefore a high-energy electron is gained at the expense of a medium energy electron and the phenomenon is consistent with the observation that the introduction into the plasma of a solution of 100 µg mL⁻¹ Na causes no overall increase in n_e in the DRT plasma. The high-energy electrons are able to ionize and excite Ca ions by direct collision, since the energy demand for Ca ionization and excitation is only 9.26 eV. Consequently, the maximum emission of Ca species occurs at lower heights in the presence of EIEs matrix than in its absence. The processes were observed in non-LTE plasmas and a detailed discussion can be found in the literature.[42]

For concentrations over 100; 150 and 350 µg mL⁻¹ Li, Na and K the emission at atomic and ionic line decreases, while at molecular bands it increases, as also observed in the SRT plasma (Figure 4). Since the depressive effects in the DRT plasma are lower, the operation in this geometry can tolerate higher amounts of EIEs, without affecting stability and analytical capability. In both plasma geometries, the magnitude of the depressive effect on atomic and ionic emission and of the increasing effect on molecular emission caused by a high EIEs concentration correlates inversely with MED assimilated with the lattice energy (kJ mol⁻¹): 842 for LiCl, 774 for NaCl and 730 for KCl).[36] In a recent study, Simon et al.[34] reported that the use of double ring electrode in DRT spaced at 60 mm eliminated the depressive matrix effects of Ca and Sr on Bi, Cu and Pb atomic emission and improved the detection limits up to 3 fold compared to SRT. Results showed also that higher the energy demand to atomize and excite analyte and matrix, the shorter must be the distance between the ring electrodes to reduce the depressive effect.

3. 3. Solute Vaporization Interference

The matrix effect of 100 µg mL⁻¹ Al as AlCl₃ on Ca emission signal for different observation heights in SRT and DRT plasmas is presented in Figure 5. The influence

of AlCl$_3$ and Al(NO$_3$)$_3$ matrices up to 500 µg mL^{-1} Al is shown in Figure 6. In both plasma geometries, Al induces a depression of emission signal of all Ca species caused by the chemical processes occurring mostly in solid phase and lesser in the gaseous one. According to the literature, the chemical interference between Al and Ca is the result of the development in solution of calcium aluminates, which generate mixed oxides (CaO · Al$_2$O$_3$ and 2CaO · Al$_2$O$_3$) with high MED and low atomization degree in the atomization source.[43,44]
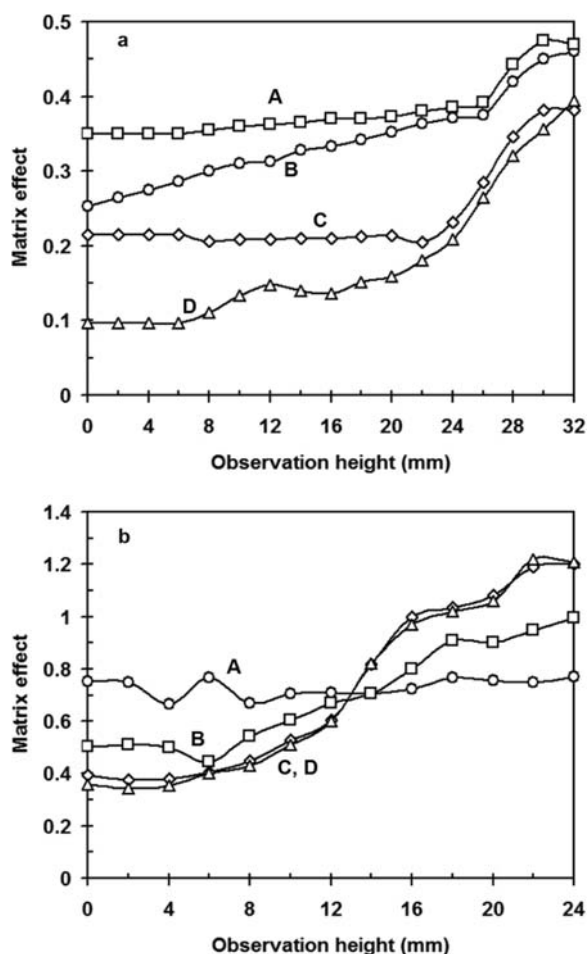

Figure 5: Matrix effect of 100 µg mL^{-1} Al as AlCl$_3$ on Ca emission *vs.* observation height in SRT plasma (a) and DRT plasma (b) for Ca II 393.367 nm (A); Ca I 422.673 nm (B); CaOH 554 nm (C) and CaOH 622 nm (D).

The development of Ca–Al compounds with volatility lower than that of the analyte translates the emission maxima of Ca species towards higher observation heights compared to those in the absence of the matrix. The depressive effect caused by secondary chemical processes in the Ca–Al mixture diminishes with increasing observation height as a result of an improved atomization efficiency of refractory compounds in accord with the enhanced temperature in plasma.
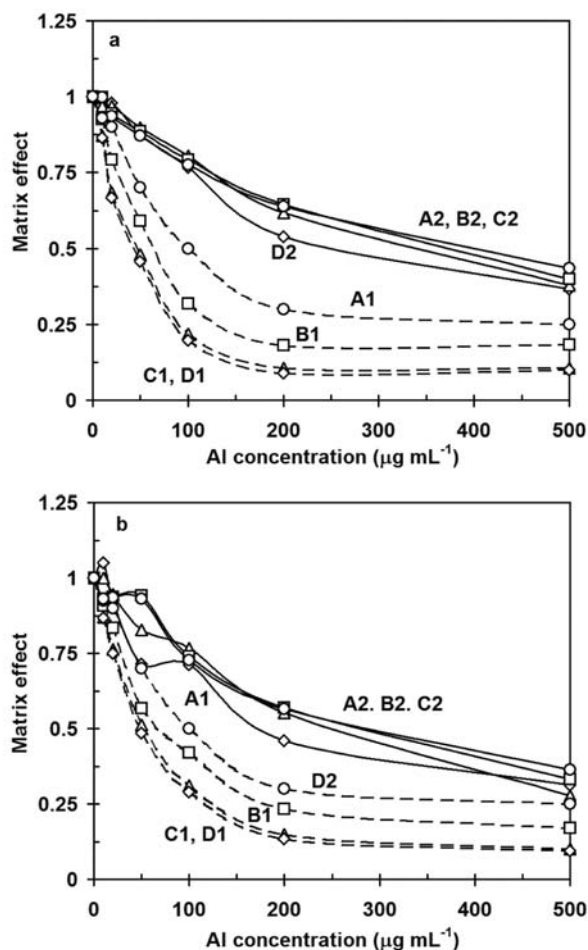

Figure 6. Effect of matrix concentration of AlCl$_3$ (a) and Al(NO$_3$)$_3$ (b) on Ca emission in SRT plasma (dotted line) and DRT plasma (solid line). A1, A2 – Ca II 393.367 nm; B1, B2 – Ca I 422.673 nm; C1, C2 – CaOH 554 nm and D1, D2 – CaOH 622 nm

Also, in the DRT plasma of higher temperature, the Al matrix effect is two times lower than in SRT, which means an improved atomization capability of plasma in two-ring electrode geometry. A similar depressive effect of Al on Ca was reported in other low power plasma sources, such as capacitively microwave plasma (CMP)[45] and microwave induced plasma (MIP),[46] insufficiently energetic to dissociate refractory compounds with high MED. In the hotter ICP the Ca–Al interference is negligible.[45]

Data have shown (Figure 6) that the chemical interferences of Al as nitrate or chloride salts on Ca emission are of comparable magnitude, meaning that the atomization processes are similar involving stages with comparable MED, as previously reported.[33]

3. 4. Figures of Merit

The limits of detection of Ca (3σ criteria) at the optimum observation height in SRT and DRT plasmas us-

Table 4: Limits of detection (LOD, 3σ criteria) for Ca determination in the absence and presence of NaCl (100 μg mL^{-1} Na), AlCl$_3$ and Al(NO$_3$)$_3$ (100 μg mL^{-1} Al).

λ (nm)	Matrix	SRT Plasma			DRT Plasma		
		LOD (ng mL^{-1})	LOD$_{matrix}$/ LOD$_{water}$	Optimum observation height (mm)	LOD (ng mL^{-1})	LOD$_{matrix}$/ LOD$_{water}$	Optimum observation height (mm)
Ca II 393.367	Water	1600	1	28	250	1	16
	NaCl	1640	1	28	210	0.84	14
	AlCl$_3$	4140	2.60	32	360	1.44	18
	Al(NO$_3$)$_3$	4230	2.65	32	370	1.48	18
Ca I 422.673	Water	310	1	24	100	1	14
	NaCl	320	1	24	100	1	10
	AlCl$_3$	775	2.50	28	145	1.45	16
	Al(NO$_3$)$_3$	790	2.55	28	145	1.45	16
CaOH 554 nm	Water	290	1	24	230	1	12
	NaCl	230	0.80	22	210	0.90	8
	AlCl$_3$	930	3.20	28	385	1.7	16
	Al(NO$_3$)$_3$	940	3.25	28	385	1.7	16
CaOH 622 nm	Water	130	1	24	100	1	12
	NaCl	106	0.80	22	92	0.92	8
	AlCl$_3$	430	3.30	28	170	1.7	16
	Al(NO$_3$)$_3$	450	3.45	28	170	1.7	16

ing the PDA multichannel spectrometer in the absence and presence of 100 μg mL^{-1} Na and Al are presented in Table 4.

The limit of detection for Ca depends on coupling geometry of the radiofrequency power to the plasma torch, nature of emitting Ca species and matrix. In the SRT geometry the best detection limit of 106–450 ng mL^{-1} Ca and the highest calibration sensitivity were achieved at CaOH 622 nm molecular band regardless the nature of the matrix. The calibration curve plotted at CaOH 622 nm over the concentration range 1–100 μg mL^{-1} Ca provided the best correlation coefficient (0.999) and a relative standard deviation of the slope of 1 %.

In the DRT plasma, the optimum working wavelength was Ca I 422.673 nm for which the best detection limit (92–145 ng mL^{-1}) was achieved. The correlation coefficient of the calibration curve plotted at this wavelength was 0.999, while the relative standard deviation of the slope 1.3 %. Within the dynamic range, the precision of Ca determination (n = 5) was 2.9–4.9 %. In the presence of AlCl$_3$ and Al(NO$_3$)$_3$, the calibration sensitivity decreased as a result of the depressive effect. In such conditions, the limit of detection increased 2.5 times at ionic and atomic lines and 3.5 times at molecular bands in the SRT geometry and only 1.5 and 1.7 times respectively, in the DRT geometry.

4. Conclusions

A complete picture of the non-spectral interferences in a medium power plasma source with single or double ring electrode due to EIEs and Al on Ca determination by OES at atomic and ionic lines and molecular bands has been established. It has been shown that the introduction of an interferent causes shifts in analyte emission maps in both plasma geometries as well as a decrease in the electron number density and gas temperature, especially in the SRT configuration. The matrix effects of EIEs and Al in the studied plasma are dependent on the coupling geometry of the rf power and the viewing height. The approach of the DRT configuration and the optimization of the observation height allowed the reduction of interferences caused by the studied matrices. The LTE model and MED apply to explain interference of high levels of EIEs, while the model fails for low concentrations. The mechanism of chemical interference of Al on Ca emission is independent from the nature of the Al species as it involves processes with similar energy demands. The studied rfCCP could be a valuable spectral source for Ca determination by OES in EIEs and Al matrices at the molecular band CaOH 622 nm in the SRT and Ca I 422.673 nm in the DRT geometry, respectively. The source is attractive in view of its low power requirements, reduced gas consumption and good stability in the presence of concentrated matrices, and can be the basis for manufacturing a cheep plasma spectrometer.

5. Acknowledgments

6. References

1. G. Cristescu, R. Grigorovici, *Annals of RPR Acad.* **1949**, *3*, 63–78.
2. M. W. Blades, *Spectrochim. Acta* **1994***, 49B*, 47–57.
3. S. D. Anghel, T. Frentiu, A. Simon, *The Open Plasma Phys. J.* **2009**, *2*, 8–16.
4. A. Bass, C. Chevalier, M. W. Blades, *J. Anal. At. Spectrom.* **2001,** *16*, 919–921.
5. J. Franzke, K. Kunze, M. Miclea, K. Niemax, *J. Anal. At. Spectrom.* **2003,** *18,* 802–807.
6. R. Guchardi, P.C. Hauser, *J. Anal. At. Spectrom.* **2003,** *18,* 1056–1059.
7. S. D. Anghel, A. Simon, T. Frentiu, *J. Anal. At. Spectrom.* **2003**, *20*, 966–973.
8. S. D. Anghel, A. Simon, T. Frentiu, *Plasma Sources Sci. T,* **2008**, *17*, 1–9.
9. V. Karanassios, *Spectrochim. Acta* **2004,** *59B*, 909–1045.
10. E. A. Cordos, S. D. Anghel, T. Frentiu, A. Popescu, *J. Anal. At. Spectrom.* **1994**, *9,* 635–641.
11. T. Frentiu, A. M. Rusu, M. Ponta, S. D. Anghel, E. A. Cordos, *Fresenius J. Anal. Chem.* **1996,** *354*, 254–255.
12. T. Frentiu, A. M. Rusu, S. D. Anghel, S. Negoescu, A. Popescu, A. Simon, E. A. Cordos, *ACH-Models in Chem.* **1999**, *136*, 119–129.
13. S. D. Anghel, T. Frentiu, A. M. Rusu, L. Bese, E. A. Cordos, *Fresenius J. Anal. Chem.* **1996,** *355*, 252–253.
14. S. D. Anghel, T. Frentiu, E. A. Cordos, A. Simon, A. Popescu, *J. Anal. At. Spectrom.* **1999**, *14*, 541–545.
15. S. Luge, J. A. C. Broekaert, *Anal. Chim. Acta* **1996,** *332*, 193–199.
16. D. Huang, M.W. Blades, *J. Anal. At. Spectrom.* **1991,** *6*, 215–219.
17. R. Gross, B. Platzer, E. Leitner, A. Schalk, H. Sinabell, H. Zack, G. Knapp, *Spectrochim. Acta* **1992**, *47B*, 95–106.
18. X. Quan, S. Chen, B. Platzer, J. Chen, M. Gfrerer, *Spectrochim. Acta* **2002**, *57B*, 189–199.
19. N. Watanabe, W. Buscher, G. Böhm, *Anal. Sci.* **2002**, *18*, 1191–1194.
20. M. M. Rahman, M. W. Blades, *Spectrochim. Acta* **2000**, *55B*, 327–338.
21. R. E. Sturgeon, S. N. Willie, V. T. Luong, S. S. Berman, *J. Anal. At. Spectrom.* **1991,** *6*, 19–23.
22. T. D. Hetipathirana, M. W. Blades, *J. Anal. At. Spectrom.* **1993,** *8*, 955–959.
23. D. L. Smith, D. C. Liang, D. Steel, M.W. Blades, *Spectrochim. Acta* **1990**, *45B*, 493–498.
24. S. Imai, R. E. Sturgeon, *J. Anal. At. Spectrom.* **1994**, *9*, 765–772.
25. F. Herwig, J. A. C. Broekaert, *Microchim. Acta* **2000,** *134*, 51–56.
26. E. A. Cordos, T. Frentiu, A. Fodor, M. Ponta, A. M. Rusu, S. Negoescu, *ACH Models in Chem.* **1995,** *132,* 313–329.
27. E. A. Cordos, T. Frentiu, A. M. Rusu, S. D. Anghel, A. Fodor, M. Ponta, *Talanta* **1999**, *48,* 827–837.
28. T.Frentiu, E. Darvasi, S. D. Anghel, A. Simon, M. Ponta, E. A. Cordos, *Chem. Anal. (Warsaw)* **2002***, 47,* 725–736.
29. E. A. Cordos, T. Frentiu, A. M. Rusu, G. Vatca, *Analyst* **1995**, *120,* 725–735.
30. T. Frentiu, M. Ponta, A. M. Rusu, S. D. Anghel, A. Simon, E. A. Cordos, *Anal. Lett.* **2000**, *33,* 323–335.
31. M. Ponta, T. Frentiu, A. M. Rusu, E. A. Cordos, *Croat. Chem. Acta* **2002**, *75,* 291–306.
32. T. Frentiu, M. Ponta, S. D. Anghel, A. Simon, I. Marginean, E. A. Cordos, *Microchim. Acta* **2003***, 143,* 245–254.
33. T. Frentiu, M. Ponta, S. D. Anghel, A. Simon, A. M. Incze, E. A. Cordos, *Microchim. Acta* **2004**, *147,* 93–103.
34. A. Simon, T. Frentiu, S. D. Anghel, S. Simon, *J. Anal. At. Spectrom.* **2005**, *20*, 957–965.
35. T. Frentiu, E. Darvasi, M. Senila, M. Ponta, E. Cordos, *Talanta*, **2008**, *76*, 1170–1176.
36. G. Niac, V. Voiculescu, I. Baldea, M. Preda: Formule, tabele, probleme de chimie fizica, Ed. Dacia, Cluj-Napoca, **1984**, pp. 143–144.
37. S. D. Anghel, T. Frentiu, A. Popescu, A. Simon, E. Cordos, *Rom. J. Optoelectron.* **1997**, *5*, 37–42.
38. Ch. De Izarra, *Int. J. Mod. Phys.* C **2000,** *11*, 987–998.
39. P. J. W. M. Boumans, F. J. De Boer, **1977,** *32B*, 365–395.
40. http://physics.nist.gov/PhysRefData/ASD/index.html. NIST: Atomic Spectra Data Base
41. D. S. Hanselman, N. N. Sesi, M. Huang, *Spectrochim. Acta* **1994**, *49B*, 495–526.
42. A. Versteegh, K. Behringer, U. Fantz, G. Fussmann, B. Juttner, S. Noack, *Plasma Sources Sci. T.* **2008**, *17*, 024014 (8pp)
43. C. R. Dockery, M.J. Blew, S. R. Goode, *J Chem. Ed* **2008**, *85*, 854–858
44. C. Th. J. Alkemade, *Anal. Chem.* **1966**, *38*, 1252–1253.
45. G. F. Larson, V. A. Fassel, *Anal. Chem.* **1976**, *48*, 1161–1166.
46. Y. Duan, X. Li, Q. Jin, *J. Anal. At. Spectrom.* **1993***, 6*, 1091–1096.

Povzetek

Preučevali smo ne-spektralne interference lahko ionizirajočih elementov (EIE) kot kloridov in Al kot AlCl$_3$ in Al(NO$_3$)$_3$, na emisijo Ca II 393,367 nm, Ca I 422,673 nm, CaOH 554 nm in 622 nm v radiofrekvenčnem kapacitivno sklopljenem argonskem plazemskem viru srednje moči (275 W, 27,12 MHz) z enojno (SRTrfCCP) in dvojno prstanasto elektrodo (DRTrfCCP). Mehanizme interference smo razložili na podlagi energijskih potreb matrice, pri čemer smo predvideli lokalno termično ravnotežje v plazmi. Opazili smo, da so učinki matrice odvisni od sklopitvene geometrije med radiofrekvenčno tuljavo in baklo, od višine opazovanja, identitete sevajočih Ca zvrsti in narave EIE matrice, hkrati pa neodvisni od izvora Al soli. Velikost učinka matrice smo korelirali z elektronsko gostoto in temperaturo razelektritve. Z optimizacijo smo lahko omejili vpliv EIE in Al, ter višine opazovanja. Najboljša meja detekcije za Ca pri SRTrfCCP je CaOH 622 nm (106–450 ng ml^{-1}), medtem ko je pri DRTrfCCP Ca I 422.673 nm (92–145 ng ml^{-1}).